Heteroatom-Modulated Switching of Photocatalytic Hydrogen and Oxygen Evolution Preferences of Anatase TiO_2 Microspheres

*Gang Liu, Jian Pan, Lichang Yin, John TS Irvine, Feng Li, Jun Tan, Philip Wormald, and Hui-Ming Cheng**

Understanding and manipulating the two half-reactions of photoinduced electron reduction and hole oxidation are key to designing and constructing efficient photocatalysts. Here, how the spatial distribution of the heteroatom modulates photocatalytic reduction (hydrogen evolution) and oxidation (oxygen evolution) reaction preferences is investigated by moving boron from the core to the shell of an anatase TiO_2 microsphere along [001] via thermal diffusion control. The preference towards photocatalytic hydrogen and oxygen producing reactions from splitting water can be switched by creating a shell with an interstitial $B^{\sigma+}$ ($\sigma \leq 3$) gradient in the TiO_2 microsphere. This switching stems from the downward shift of electronic band edges of the shell by a band bending effect that originates from the extra electrons coming from the interstitial $B^{\sigma+}$. These results create new opportunities for designing and constructing efficient photocatalysts by spatial heteroatom engineering.

1. Introduction

Semiconductor photocatalysts have attracted increasing attention due to their great potential in applications of clean environment and renewable energy.[1–18] The synergistic effects of two half-reactions of photoinduced electron-reduction and hole-oxidation, i.e. important hydrogen and oxygen evolutions from water splitting, inherently determine photocatalysis efficiency.[19,20] Although it is well recognized that the efficiency of a photocatalyst is very sensitive to its electronic structure, the effect of the changes in electronic structure on tuning photoreaction preferences is far from well understood and utilized. Introducing heteroatoms into photocatalysts has long been used to modulate the electronic structure of photocatalysts with an overwhelming purpose of increasing visible light absorption through narrowing the bandgap or forming localized states in the bandgap.[4,21–28] In this respect, the electronegativity and ionic radius, chemical state and spatial distribution of heteroatoms are the basic parameters of major concern. To date, several encouraging advances have stimulated the rapid development of heteroatom doping in photocatalysts towards efficient utilization of visible (solar) light;[4,21–25] however, the underlying role of heteroatom in fine-tuning the photocatalytic reaction preferences has been unfortunately overlooked and is little understood. Developing the ability of manipulating photoreaction preferences will be critically important for designing and constructing efficient photocatalysts for targeted reactions.

The prerequisite to examine the true effects of heteroatom on photoreaction preference is to obtain a suitable photocatalyst that satisfies at least the following criteria: 1) the ability to host sufficient heteroatoms without changing the crystal structure, morphology and particle size of the photocatalyst so that the role of heteroatom can be well revealed; 2) controllable diffusion of the heteroatom in the bulk crystal along some certain crystal orientations, which makes it possible to manipulate heteroatom locations. However, heteroatoms in most photocatalysts, e.g. typical TiO_2, usually prefer to locate in the surface/subsurface area of a particle as a result of the poor diffusion ability and/or low thermodynamic solubility of heteroatoms,[27,28] particularly for those prepared by wet-chemistry routes. Therefore, it remains a great challenge to obtain a suitable candidate for studying the effects of heteroatoms on photoreaction preference.

Among the intensively investigated nonmetal dopants, boron[29] which has the smallest ionic radius might be an ideal candidate to be accommodated and diffuse within bulk TiO_2 under an external driving force. Inspired by the preparation of TiO_2 polymorphs from crystalline TiB_2 with H_3BO_3 as a by-product,[30] in this work we proposed an oriented agglomeration growth strategy to in situ synthesize TiO_2 microspheres containing B dopant, as illustrated in **Figure 1**a and Figure S1 (Supporting Information). By controlling the spatial distribution of boron, the effect and its origin of the heteroatom on modulating photocatalytic reaction preferences towards hydrogen

Dr. G. Liu, J. Pan, Dr. L. C. Yin, Dr. F. Li, Dr. J. Tan, Prof. H.-M. Cheng
Shenyang National Laboratory for Materials Science
Institute of Metal Research
Chinese Academy of Sciences
72 Wenhua RD, Shenyang 110016, China
E-mail: cheng@imr.ac.cn
Prof. J. TS Irvine, Dr. P. Wormald
School of Chemistry
University of St. Andrews
Fife, KY16 9ST, UK

DOI: 10.1002/adfm.201200414

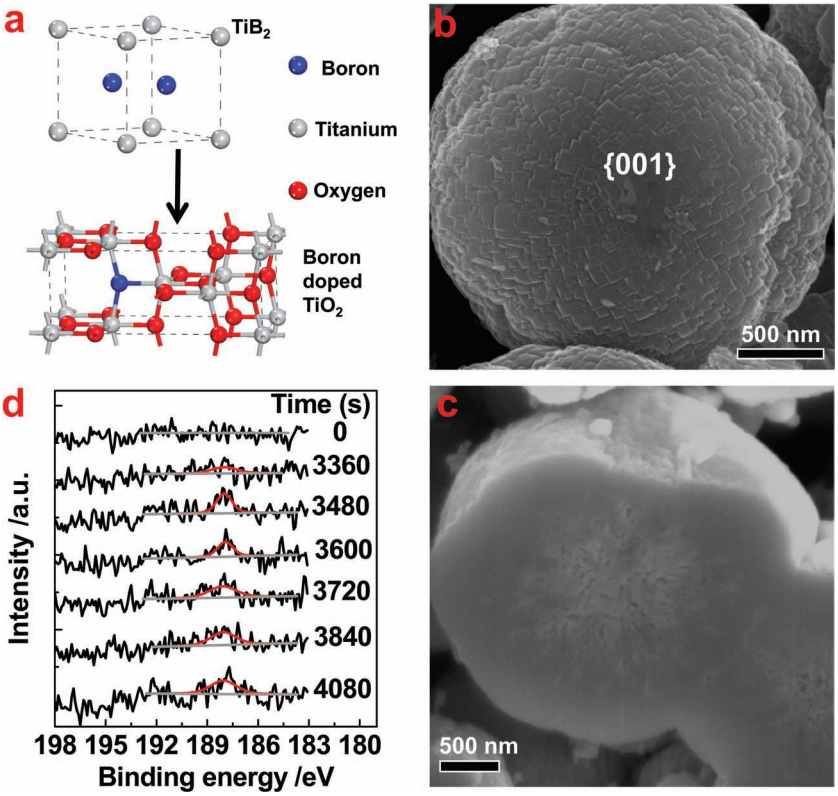

Figure 1. The morphology and inner structure of an anatase TiO_2 microsphere. a) Crystal structures of hexagonal TiB_2 and anatase tetragonal TiO_2. b) Scanning electron microscopy (SEM) image of a prepared anatase TiO_2 microsphere. c) A secondary SEM cross-sectional image of an anatase sphere after cutting by focused ion beam (FIB). d) Argon ion sputtering dependent XPS spectra of B 1s from the TiO_2 microspheres before thermal treatment.

and oxygen evolution from splitting water were demonstrated. The results obtained provide some important implications in designing and constructing efficient photocatalysts.

2. Results and Discussion

2.1. Morphology and Structure of TiO_2 Microspheres

X-ray diffraction analyses (Figure S2, Supporting Information) confirm that the final sample synthesized from TiB_2 is 94.5 wt% anatase and 5.5 wt% rutile TiO_2. Representative SEM image of the sample shows that most TiO_2 particles appear as well-developed spheres with a predominant diameter of 2–4 μm (Figure S3, Supporting Information). Furthermore, both anatase and rutile phases tend to agglomerate separately as indicated in Figure S4 (Supporting Information). The surface of the anatase microsphere in Figure 1b consists of nanosized truncated pyramids with the top major {001} and lateral minor {101} facets as characterized by Figure S5 (Supporting Information).[31,32] The cores of the spheres shown in Figure 1c are partially hollowed as a result of the well-known Oswald ripening process during crystal growth.[33] The morphology, crystal phase and size of these microspheres show no detectable change after calcination at 600 °C in air for 2 h. Inductively coupled plasma (ICP) atomic emission spectrometry measurements verify the unchanged amount of boron at ca. 1.1 at% (B/Ti) in the microspheres upon calcination.

2.2. Distribution and Chemical States of Boron in the Microspheres

The distribution and chemical state of boron in the TiO_2 microspheres was investigated with X-ray photoelectron spectroscopy (XPS). Prior to the thermal treatment, boron is absent from the surface layer of the microsphere shell, as indicated by the absence of an XPS B 1s signal before 3360 s Ar^+ sputtering in Figure 1d. Boron with its B 1s level binding energy at 187.9 eV, identified as substitutional boron ($B^{\delta-}$, $\delta \leq 2$) to replace lattice oxygen to form Ti-B bond,[29] exists in the core of microsphere. After the thermal treatment, a boron gradient, with a maximum content at the outer surface (**Figure 2**a) is formed in the shell as a result of thermal diffusion of boron from the core to the shell (The shell thickness is estimated to be around 50 nm.). Furthermore, the B 1s level binding energy detected in the shell increases from 187.9 eV to 192.2 eV, thus suggesting a conversion from the substitutional boron $B^{\delta-}$ to interstitial boron ($B^{\sigma+}$, $\sigma \leq 3$),[29] caused by heating. Such conversion is consistent with the theoretical results that the substitutional boron is much less stable than the interstitial boron, and even the displacement of the boron atom from the substitutional to the interstitial position has a net cost with a sufficiently high temperature.[34] The evolution of boron distribution in the TiO_2 microsphere upon heating is illustrated in Figure 2b. The detailed chemical coordination environment of the boron in TiO_2 was clarified by solid state nuclear magnetic resonance (NMR) spectroscopy. Consistent with XPS results, the NMR spectrum of ^{11}B in TiO_2 with substitutional boron shows different features from that in TiO_2 with the interstitial boron due to different chemical environments of boron (Figure 2c). Due to the fact that all bulk lattice oxygen atoms have a threefold coordination ([OTi_3]),[34] the chemical shift of the dominant signal at −1.88 ppm, therefore, should correspond to substitutional boron coordinated in trigonal unit [BTi_3]. Two kinds of interstitial boron, which are coordinated in tetragonal and trigonal units [BO_4] and [BO_3], may exist in anatase TiO_2.[34] In this case, the dominant signal at 1.72 ppm and the minor shoulder signal originate from the interstitial boron coordinated in [BO_4] and [BO_3] units, respectively.[35] It is worth noting that the interstitial B in both units theoretically plays the same role in changing the electronic structures of TiO_2.[34]

2.3. Electronic Band Structures of the Anatase TiO_2 Microsphere

We investigated the effect of boron on electronic structure of TiO_2 by combining UV-visible absorption spectroscopy with XPS

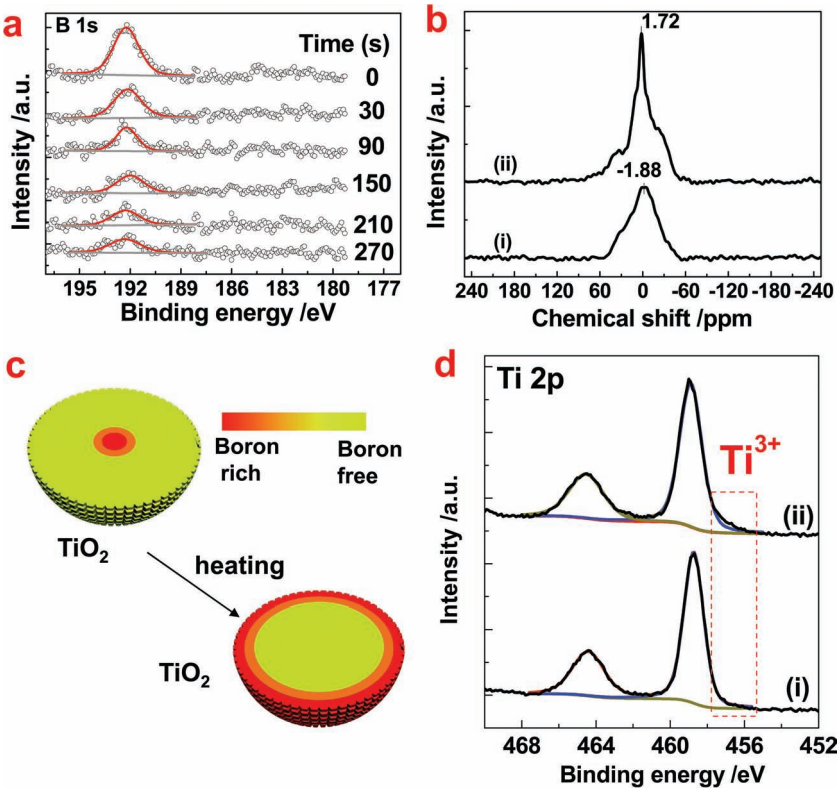

Figure 2. Gradient distribution of boron within the TiO_2 microspheres and chemical state of Ti. a) Argon ion sputtering dependent XPS spectra of B from the TiO_2 microspheres after thermal treatment. b) Schematic of the evolution of boron distribution within an anatase microsphere upon heating. c) Solid state NMR spectra of ^{11}B recorded from the TiO_2 microspheres i) before and ii) after thermal treatment. d) Ti 2p X-ray photoelectron spectra recorded from the pristine surface of the TiO_2 microspheres i) before and ii) after thermal treatment.

valence band spectroscopy. The overlapping absorption edges in Figure S6 (Supporting Information) suggest that the intrinsic bandgap is independent of the chemical states of boron. This is consistent with the reported theoretical results that both interstitial and substitutional boron lead to no change in the intrinsic bandgap of anatase TiO_2.[34] However, the valence band maximum of the shell containing interstitial boron is apparently shifted downwards by 0.26 eV from 1.98 eV to 2.24 eV with respect to the boron-free shell (Figure S7, Supporting Information). The origin of the downward shift is attributed to the known band bending effect caused by the extra electrons from donor defects,[36] Ti^{3+} in this case. Introducing interstitial boron in TiO_2 will cause the formation of Ti^{3+} by contributing valence electrons from boron to a neighboring Ti^{4+}, according to the following defect equation: $B + Ti^{4+} \rightarrow 1/\sigma\ B^{\sigma+}$ ($\sigma \leq 3$) + Ti^{3+}.[34,35] The existence of Ti^{3+} is validated by the appearance of an additional shoulder from 457.6 eV to 456.0 eV in XPS spectrum of Ti 2p (Figure 2d), which is formally assigned to Ti^{3+}.[36] Based on these results, the respective surface band structure of the boron-free and boron containing shell is illustrated in **Figure 3**a. The bulk electronic structure of the whole shell with a boron gradient can be then mapped from the surface electronic structure in Figure 3b. The basis of this mapping is the linked distribution of $B^{\sigma+}$ with that of Ti^{3+} due to the coexistent relationship of Ti^{3+} with $B^{\sigma+}$.

2.4. Photocatalytic Activities

We now estimate how the boron-dependent spatial electronic structure affects the photocatalytic reduction and oxidation reactions first by monitoring hydrogen and oxygen evolution from water splitting in the presence of methanol and $AgNO_3$ as electron and hole donors,[8,10,15] respectively. As shown in **Figure 4**, the boron-free shell leads to a 4-fold improvement in hydrogen evolution compared to the shell with a boron gradient. However, the boron-containing shell results in a 4.5-fold improvement in oxygen evolution compared to the shell with a boron gradient. That is, the boron introduced in the shell has a totally opposite effect on the hydrogen and oxygen evolution from water splitting. Photocatalysis requires a simultaneous occurrence of reduction and oxidation induced by the photoexcited conduction band electrons and valence band holes, respectively. In the presence of an electron (hole) donor that easily consumes the photoexcited holes (electrons), the activity of splitting water to produce hydrogen (oxygen) by the photoexcited electrons (holes) as the rate-limiting step is determined by the redox power of the electrons (holes). As indicated in Figure 3b, the electrons from the boron-free shell have a stronger reducing power than those from the shell with a boron gradient, while the holes from the latter have a stronger oxidative power than those from the former. This can well explain the hydrogen and oxygen

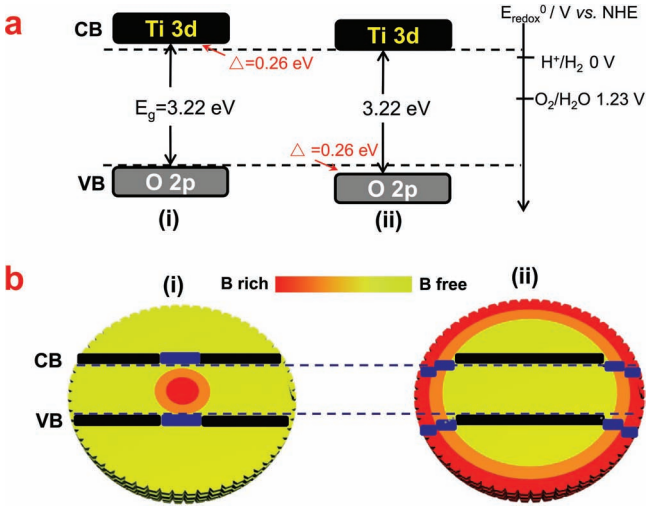

Figure 3. Boron distribution-dependent electronic structure. a) Surface band structure alignments of the TiO_2 microspheres. b) The dependence of spatial electronic structures on the distribution of boron within the TiO_2 microspheres. The bands in the boron containing areas are highlighted in blue. i) TiO_2 microspheres with a boron-free shell and ii) TiO_2 microspheres with a boron-containing shell.

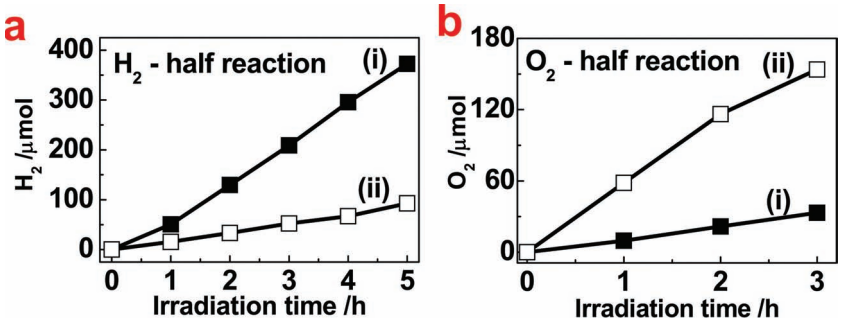

Figure 4. Boron distribution-dependent photocatalytic activities. a) Photocatalytic hydrogen evolution from 1 wt% Pt loaded TiO_2 microsphere photocatalysts in the presence of methanol as an electron donor. b) Photocatalytic oxygen evolution from the TiO_2 microsphere photocatalysts in the presence of $AgNO_3$ as a hole donor: i) TiO_2 microspheres with a boron-free shell and ii) TiO_2 microspheres with a boron-containing shell.

evolution preference of the TiO_2 microspheres by introducing boron in the shell.

2.5. Diffusion Behaviors of Boron in the Microsphere

The above photocatalytic behaviors are modulated by the heteroatom of boron moving from the core to the shell within a microsphere. Further in-depth understanding of boron diffusion within a TiO_2 structure framework on a microscopic scale is, therefore, desirable, and was studied by monitoring the electrical conduction characteristics of a single microsphere. *I–V* curves, which were recorded from a single microsphere (Insets in **Figure 5**a,b), clearly demonstrate a direct dependence of electrical conduction characteristics on the boron distribution. Independent of scanning times and direction, the microsphere with boron in the shell shows the typical electron conduction behavior of an ordinary semiconductor due to the highly diluted distribution of interstitial boron in the whole shell (Figure 5a). However, for a microsphere with boron in the core, a cooperative conduction of an electron and a $B^{\sigma+}$ ion (applied electronic field will act as the thermal field in converting substitutional $B^{\delta-}$ to interstitial $B^{\sigma+}$ before starting boron diffusion as indicated by the facile conversion in Figure S8, Supporting Information) emerges in the first scanning, but then electron conduction alone appears in the second and the following scans, under the applied increasing voltages (Figure 5b). This phenomenon can be well explained in terms of the occurrence of a directional diffusion of concentrated $B^{\sigma+}$ ions within the microsphere along the electric field, as illustrated in Figure 5c. The exact contribution of $B^{\sigma+}$ ion conduction to the electrical conductivity, derived by subtracting the 1st (3rd) curve from the 2nd (4th) in Figure 5a,b, is indicated by the dash lines. Two important features are observed from Figure 5b: i) an extremely low threshold voltage for the transport of $B^{\sigma+}$; ii) the maximum ion conductivity appearing at ca. ±3 V as a cooperative effect of the applied electrical field and the amount of available $B^{\sigma+}$ ions in the bulk for the transport.

We further tried to understand the interstitial boron diffusion behavior at the atomic level by theoretically revealing possible diffusion pathways between two nearest $[BO_4]$ sites along the anatase [001] orientation. As shown in Figure 5d, the most energetically preferable pathway for interstitial B was calculated to be $[BO_4]_{IS} \rightarrow [BO_3]_a^1 \rightarrow [BO_3]_a^2 \rightarrow [BO_4]_{FS}$ with a moderate energy barrier (1.76 eV), which is much less than those (3.69 eV and 3.16 eV) calculated for other two pathways $[BO_4]_{IS} \rightarrow [BO_3]_a^1 \rightarrow [BO_3]_b^1 \rightarrow [BO_4]_{FS}$ and $[BO_4]_{IS} \rightarrow [BO_3]_b^2 \rightarrow [BO_3]_a^2 \rightarrow [BO_4]_{FS}$ (Figure S9, Supporting Information). This moderate barrier can well explain the high diffusion capability of boron under the driving force of both the applied thermal field and electric field.

3. Conclusions

We report a heteroatom-modulated switching of photocatalytic reaction preference towards hydrogen or oxygen producing reaction from water splitting with boron contained anatase TiO_2 microspheres. This switching is sensitively controlled by creating a shell with an interstitial $B^{\sigma+}$ ($\sigma \leq 3$) gradient in the TiO_2 microsphere. Such a modulating effect intrinsically stems from the downward-shift of electronic band edges of the shell by a band bending effect caused by the extra electrons coming from the interstitial $B^{\sigma+}$. The results achieved clearly demonstrate the strong capability of heteroatom in modulating photocatalytic reaction preference of photocatalysts. The findings open up new opportunities for developing photocatalysts with tunable photoreaction preferences based on spatial heteroatom engineering.

4. Experimental Section

Synthesis of the TiO_2 Microspheres: Sodium sulfate (Na_2SO_4, Aldrich Chemical) was dissolved in 1 M hydrochloric acid (HCl) to a concentration of 0.11 M. In a typical synthesis procedure, 55 mg of titanium diboride (TiB_2) was then added into 12 mL of the above aqueous solution to form a dark grey suspension. The suspension was transferred to a Teflon-lined autoclave and heated at 180 °C for 24 h. A white suspension containing the sample was obtained after the reaction. The sample was collected by centrifugation and fully washed with deionized water to remove any dissolvable impurity. The sample was finally dried at 80 °C in air for further characterization.

Tuning the Distribution of Boron in the Microspheres: In order to move the boron from the core to the shell of the resultant TiO_2 microspheres, the sample obtained from the above procedure was heated at 600 °C in air for 2 h with a heating rate of 5 °C/min. The sample was cooled to room temperature naturally.

Processing the Microspheres by a Focused Ion Beam (FIB): The processing of TiO_2 microspheres were performed in a FIB workstation (Nova 200, Nanolab) using a liquid metal ion source to generate ions (typically Ga^+) to sputter specimens. The Ga^+ ions were accelerated at a high voltage (typically 30 kV) to sputter the TiO_2 microsphere. Thereby, a cross section of the TiO_2 microspheres was obtained.

Photocatalytic Activity Measurements: Photocatalytic hydrogen and oxygen evolution reactions were carried out in a top-irradiation vessel connected to a glass-enclosed gas circulation system. 100 mg of the TiO_2 powder was dispersed in 300 mL aqueous solution containing 10 vol% methanol for hydrogen evolution or 16.7 mM $AgNO_3$ for oxygen evolution. The reaction temperature was maintained around

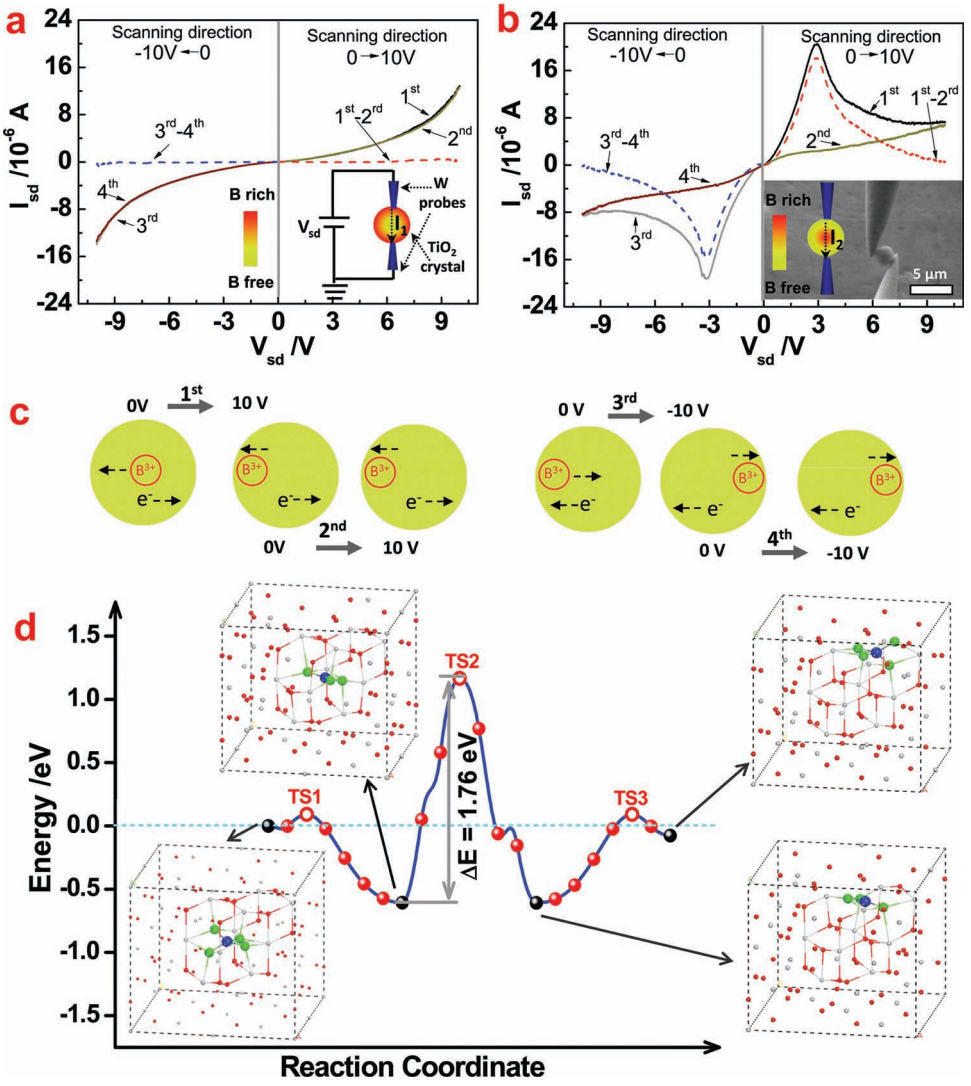

Figure 5. Diffusion characteristics of boron within anatase TiO_2. a,b) *I–V* curves measured from a single anatase TiO_2 microsphere with a boron containing and boron-free shell, respectively. The 1st, 2nd, 3rd, 4th curves were recorded in turn, where the 1st and 2nd were scanned from 0 V to 10 V, while the 3rd and 4th were subsequently scanned from 0 V to -10 V. The dashed lines were derived by subtracting the 1st and 3rd curves from the 2nd and 4th curves, respectively. c) Proposed directional boron diffusion processes in the microsphere with initial boron in the core under different measurement conditions. d) Calculated minimum energy path for the most energetically preferable interstitial boron diffusion along [001] in bulk anatase. Three possible locations for the interstitial boron in bulk anatase, including two 3-coordinated $B^{\sigma+}$, ($[BO_3]_a$ and $[BO_3]_b$, where a, b indicate two different configurations) and one 4-coordinated $B^{\sigma+}$ ($[BO_4]$) configurations, were considered according to ref. [34]. The structures for the initial state $[BO_4]$ ($[BO_4]_{IS}$), local state $[BO_3]_a^1$ and $[BO_3]_a^2$ (1, 2 indicating two equal sites of $[BO_3]$), and final state $[BO_4]$ ($[BO_4]_{FS}$) are also presented. TS: transition state. Small red and grey balls indicate O and Ti atoms, $[BO_4]$ and $[BO_3]$ groups are highlighted by large green (O) and blue (B) atoms.

20 °C. The amount of H_2 and O_2 evolved was determined using a gas chromatograph (Agilent Technologies: 6890N).

Details of theoretical calculations, electrical property measurement of a single anatase microsphere are given in Supporting information.

Supporting Information

Supporting Information is available from the Wiley Online Library or from the author.

Acknowledgements

The authors thank Mr. C. Zhen for the valuable discussion on $B^{\sigma+}$ ion conduction, Ms. P. Niu, Mr. Y. P. Xie, Mr. W. Jiao for their assistance with photoreactivity measurements, Dr. P. F. Yan and Mr. J. W. Deng for their assistance with TEM characterization. The authors acknowledge gratefully the financial support from the Major Basic Research Program, Ministry of Science and Technology of China (No. 2009CB220001), NSFC (Nos. 50921004, 51002160, 21090343), and the Solar Energy Initiative of the Chinese Academy of Sciences. L.C.Y. acknowledges the grants from Informalization Construction Project of CAS (No.INFO-115-B01) and the GPU project of MOF (No. ZDYZ2008-2-A12), China. G.L. acknowledges the Institute of Metals Research and Shenyang National Laboratory for Materials Science for the T.S. Kê Fellowship.

Received: February 10, 2012
Published online: April 23, 2012

[1] A. Fujishima, K. Honda, *Nature* **1972**, *238*, 37.
[2] T. Inoue, A. Fujishima, S. Konishi, K. Honda, *Nature* **1979**, *277*, 637.
[3] M. Grätzel, *Nature* **2001**, *414*, 338.
[4] Z. G. Zou, J. H. Ye, K. Sayama, H. Arakawa, *Nature* **2001**, *414*, 625.
[5] K. Maeda, K. Teramura, D. L. Lu, T. Takata, N. Saito, Y. Inoue, K. Domen, *Nature* **2006**, *440*, 295.
[6] K. Maeda, K. Domen, *Chem. Mater.* **2010**, *22*, 612.
[7] H. Tada, T. Mitsui, T. Kiyonaga, T. Akita, K. Tanaka, *Nat. Mater.* **2006**, *5*, 782.
[8] A. Kudo, Y. Miseki, *Chem. Soc. Rev.* **2009**, *38*, 253.
[9] H. Tada, T. Kiyonaga, S. Naya, *Chem. Soc. Rev.* **2009**, *38*, 1849.
[10] X. C. Wang, K. Maeda, A. Thomas, K. Takanabe, G. Xin, J. M. Carlsson, K. Domen, M. Antonietti, *Nat. Mater.* **2009**, *8*, 76.
[11] Z. G. Yi, J. H. Ye, N. Kikugawa, T. Kako, S. X. Ouyang, H. Stuart-Williams, H. Yang, J. Y. Cao, W. J. Luo, Z. S. Li, Y. Liu, R. L. Withers, *Nat. Mater.* **2010**, *9*, 559.
[12] X. Q. Gong, A. Selloni, M. Batzill, U. Diebold, *Nat. Mater.* **2006**, *5*, 665.
[13] J. G. Tao, T. Luttrell, M. Batzill, *Nat. Chem.* **2011**, *3*, 296.
[14] M. Law, L. E. Greene, J. C. Johnson, R. Saykally, P. D. Yang, *Nat. Mater.* **2005**, *4*, 455.
[15] X. B. Chen, S. H. Shen, L. J. Guo, S. S. Mao, *Chem. Rev.* **2010**, *110*, 6503.
[16] E. Martínez-Ferrero, Y. Sakatani, C. Boissière, D. Grosso, A. Fuertes, J. Fraxedas, C. Sanchez, *Adv. Funct. Mater.* **2007**, *17*, 3348.
[17] A. I. Hochbaum, P. D. Yang, *Chem. Rev.* **2010**, *110*, 527.
[18] H. Tada, M. Fujishima, H. Kobayashi, *Chem. Soc. Rev.* **2011**, *40*, 4232.
[19] M. R. Hoffmann, S. T. Martin, W. Y. Choi, D. W. Bahnemann, *Chem. Rev.* **1995**, *95*, 69.
[20] A. L. Linsebigler, G. Q. Lu, J. T. Yates Jr., *Chem. Rev.* **1995**, *95*, 735.
[21] W. Choi, A. Termin, M. R. Hoffmann, *J. Phys. Chem.* **1994**, *98*, 13669.
[22] H. J. Queisser, E. E. Haller, *Science* **1998**, *282*, 945.
[23] R. Asahi, T. Morikawa, T. Ohwaki, K. Aoki, Y. Taga, *Science* **2001**, *293*, 269.
[24] S. U. M. Khan, M. Al-Shahry, W. B. Ingler, *Science* **2002**, *297*, 2243.
[25] X. B. Chen, L. Liu, P. Y. Yu, S. S. Mao, *Science* **2011**, *331*, 746.
[26] T. L. Thompson, J. T. Yates Jr., *Chem. Rev.* **2006**, *106*, 4428.
[27] N. Serpone, *J. Phys. Chem. B* **2006**, *110*, 24287.
[28] G. Liu, L. Z. Wang, H. G. Yang, H. M. Cheng, G. Q. Lu, *J. Mater. Chem.* **2010**, *20*, 831.
[29] W. Zhao, W. H. Ma, C. C. Chen, J. C. Zhao, Z. G. Shuai, *J. Am. Chem. Soc.* **2004**, *126*, 4782.
[30] G. Liu, H. G. Yang, C. H. Sun, L. N. Cheng, L. Z. Wang, G. Q. Lu, H. M. Cheng, *CrystEngComm* **2009**, *11*, 2677.
[31] H. G. Yang, C. H. Sun, S. Z. Qiao, J. Zou, G. Liu, S. C. Smith, H. M. Cheng, G. Q. Lu, *Nature* **2008**, *453*, 638.
[32] G. Liu, J. C. Yu, G. Q. Lu, H. M. Cheng, *Chem. Commun.* **2011**, *47*, 6763.
[33] H. G. Yang, H. C. Zeng, *J. Phys. Chem. B* **2004**, *108*, 3492.
[34] E. Finazzi, C. Di Valentin, G. Pacchioni, *J. Phys. Chem. C* **2009**, *113*, 220.
[35] N. D. Feng, A. Zheng, Q. Wang, P. P. Ren, X. Z. Gao, S. B. Liu, Z. R. Shen, T. H. Chen, F. Deng, *J. Phys. Chem. C* **2011**, *115*, 2709.
[36] U. Diebold, *Surf. Sci. Rep.* **2003**, *48*, 53.